Links between annual surface temperature variation and land cover heterogeneity for a boreal forest as characterized by continuous, fibre-optic DTS monitoring

Kazuyuki Saito[1,2], Go Iwahana[2], Hiroki Ikawa[3], Hirohiko Nagano[2], Robert Busey[2]

[1]Japan Agency for Marine-Earth Science and Technology, Yokohama, 236-0001, Japan
[2]International Arctic Research Center, University of Alaska Fairbanks, Fairbanks, Alaska 99775, U.S.A.
[3]National Institute for Agro-Environmental Sciences, Tsukuba, 305-8604, Japan

Correspondence to: Kazuyuki Saito (ksaito@jamstec.go.jp)

Abstract. A fibre-optic DTS (distributed temperature sensing) system using Raman-scattering optical time domain reflectometry was deployed to monitor a boreal forest research site in the interior of Alaska. Surface temperatures range between -40º C in winter to 30º C in summer at this site. In parallel experiments, a fibre-optic cable sensor system (multi-mode, GI50/125, dual core; 3.4 mm) monitored at high-resolution (0.5-metre intervals at every 30 minutes) ground surface temperatures across the landscape. In addition ~~and~~, ~~at several points~~ a high resolution vertical profile ~~from~~ was acquired one-metre height above the upper subsurface ~~to a meter above.~~. The total cable ran 2.7 km with about 2.0 km monitoring a horizontal surface path. Sections of the cable sensor were deployed in vertical coil configurations (1.2 m high) to measure ~~vertical~~ temperature profiles from the ground up at 5-mm intervals. Measurements were ~~collected~~ made continuously over a ~~two~~ two-year interval from October, 2012 to October, 2014. Vegetation ~~of~~ at the ~~overall~~ site (Poker Flat Research Range) consists primarily of black spruce underlain by permafrost. Land cover types within the study area were classified into six descriptive categories: relict thermokarst lake, open moss, shrub, deciduous forest, sparse conifer forest, and dense conifer forest. The horizontal temperature data exhibited spati~~o~~-al and temporal ~~patterns~~ changes within the observed diurnal and seasonal variations. Differences in snow pack evolution and insulation effects co-varied with the land cover types. The apparatus used to monitor vertical temperature profiles generated high-resolution (c. 5 mm) data for air column, snow cover, and ground surface. This research also identified several technical challenges ~~of~~ in deploying and maintaining a DTS system ~~in~~ under sub-arctic environments.

1 Introduction

Under the current climate conditions, boreal forest regions function as major carbon sinks (IPCC, 2013; Euskirchen et al., 2006; Piao et al., 2008; Ohta et al., 2008). Taiga regions however ~~can show~~reveal considerable variations (heterogeneity) in

land cover, hosting both dense and sparse forests, shrubs, grasses, open mosses, and bare ground. Depending on their structural features and seasonal variations, each of these land cover types behaves differently in terms of energy, mass, and momentum exchange. These factors include presence of and variation in different forms of canopy, aerodynamic and radiative characteristics, phenology and snow pack, all of which can influence geothermal flux, subsurface physical conditions, and microbial activity (Euskirchen et al., 2006; Pomeroy et al., 2008; Essery et al., 2009; Rutter et al., 2009; Kasurinen et al., 2014; Ikawa et al., 2015; Purdy et al., 2016). For boreal forests, surface and subsurface conditions are critical causal variables, especially in terms of their spatio-temporal variations. Surface heterogeneity can also exert non-linear influence on energy, mass, and momentum exchange with the atmosphere (Vrese et al., 2016; Sellers, 1999). In-situ field measurements can help quantify spatio-temporal temperature patterns and help constrain numerical eco-climatic models for taiga regions. Data ~~like that~~ presented and interpreted below thus offer specific empirical information about taiga environments and contribute to larger-scale predictions by numerical eco-climate models concerning impacts of Earth's warming climate (e.g., Beer et al., 2007; Sato et al., 2016).

Distributed temperature sensing (DTS) systems perform multi-sensor monitoring of an area using a fibre-optic cable configuration ~~and Raman scattering techniques~~. Developed in the 1980s and improved thereafter, DTS was initially used in built environments, providing fire detection for example in industrial complexes ~~or~~ and power plants (Dakin et al., 1985; Dyer et al., 2012; Soto et al., 2016). The technique was subsequently adapted for hydrological and geophysical research seeking to measure temperature variations in natural environments (Selker et al., 2006a, 2006b; Tyler et al., 2009; Thomas et al., 2012; Lutz et al., 2012). The research described here represents for the first time how the method has been used to study thermal environments of a boreal forest. DTS monitoring techniques, which can provide continuous, high-resolution data, are ideal for studying ~~Large~~ seasonal variations in ambient temperatures (from -40º C in winter to 30º C in summer) and other conditions (persistent snow cover with deep hoar or ice layers, freeze / thaw cycles) that characterize interior parts of~~,~~ continental boreal forests ~~recommend these environment to DTS monitoring, which can provide continuous, high resolution data~~. The data described here include temperature variations and snow pack evolution ~~that reflect~~in ~~the~~ heterogeneous land cover of the boreal forest, and also a high resolution vertical profile of the interval from the ~~upper subsurface~~ground to ~~a~~ one-~~meter~~ metre above the surface.

Section 2 describes the research site and methodology. Section 3 describes temperature data acquired during the two-year experiment ~~results~~ for selected ~~the~~ horizontal (~~sections~~ Sects. 3.1, 3.2) and vertical (~~section~~ Sect. 3.3) targets ~~temperature data from the two-year experiment~~. Section 4 considers technical challenges of using DTS systems in sub-arctic environments and section 5 summarizes the study.

2 Methodology

2.1 Site

The Poker Flat Research Range (65˚07'24" N, 147˚29'15" W, 210 m a.s.l.) is a ~~research~~ facility managed by the University of Alaska Fairbanks (UAF) and located in the Interior of Alaska, about 50 km northeast of Fairbanks (Fig. 1). The general area is part of a discontinuous permafrost zone but the site itself is underlain by permafrost with active layer thickness of about 50 to 150 cm (Nakai et al., 2013). The research site includes an observation tower built in 2010 as part of a collaboration (known as JICS) between the Japan Agency for Marine-Earth Science and Technology (JAMSTEC) and UAF's International Arctic Research Center (IARC) (Sugiura et al., 2011; Nakai et al., 2013; Ikawa et al., 2015 ; Nagano et al., 2018). ~~The~~ This ~~JICS~~ observation tower was used for ~~to~~ making discrete~~ly~~ measurements of air temperatures at 1.5-m height, ~~downward~~ short-wave radiation measurements at 16-m height (tower top), and snow depth using an ultra-sonic sensor. The data from these sources were integrated into 30-minute intervals prior to analysis. Measurements were conducted for a period of two years, from October 13, 2012 to October 13, 2014.

A ~2.7 km fibre~~-~~optic cable was installed at the site (indicated by black line in Fig. 2a). The line traversed an ~~arcuate~~irregular~~,~~ 2 km long path and included five different stations (numbered 1-5) ~~consisting of~~with vertical temperature sensing ~~apparatus~~ equipment (see Sect. 2.2). The site's dominant vegetation type is black spruce, but locally, the site exhibits considerable variation in surface conditions and vegetation types (see Fig. 2a). We classified land cover into six descriptive categories by applying a supervised classification algorithm (Maximum Likelihood) to RGB aerial imagery, collected on September 4, 2012. Land cover designations include~~d~~ relict thermokarst, lake/bare ground, open moss, shrub, deciduous forest, sparse conifer forest, and dense conifer forest. The Majority Filter tool (ArcGIS 10.3) was applied to reduce effects of speckle noise prior to classification. Figure 2b shows the occurrence frequencies of the six land cover types along the length of the cable.

Figure 2c shows land cover type associations along with radiative and structural canopy characteristics for each measurement segment (~50-cm intervals) along the cable. The Normalized Difference Vegetation Index (NDVI) was derived from a GeoEye1 image taken on September 25, 2010. The canopy rate, the upper sight ratio covered by vegetation canopy when projected on a hemisphere, was calculated from a series of semi-spherical pictures taken at a height of 30 cm for every 70 cm along the cable by a THETA fish-eye camera (RICOH, Inc. Cylindrical projection). Ellipses are colour-coded for each land cover type and drawn with radii representing the standard deviation in canopy rate (horizontal) and NDVI (vertical).

Figures 2d - 2i shows typical ambient conditions for each land cover type. Relict thermokarst lake areas (Fig. 2d) ~~for example~~ include grassy depressions or flats once occupied by lakes formed by subsidence due to melting of ground ice from permafrost. This category also includes easily discernible bare grounds cleared by human activity~~s~~. Open moss areas (Fig. 2e) consist of open spaces covered by moss (mainly sphagnum moss, *Sphagnum fuscum*, and feather moss, *Hylocomium splendens*) or lichens, ~~with~~ where trees are absent. Shrub areas (Fig. 2f) are covered by dwarf to tall ~~shrubs~~species. Deciduous forest land cover (Fig. 2g) consists of mixed forests with deciduous (birch, aspen, willow, etc.), and conifer (black spruce, *Picea mariana*, and white spruce, *Picea glauca*) species. The sparse conifer (Fig. 2h) and dense conifer (Fig. 2i) forest land cover types are

occupied by spruces of varying density. The forest floors are mainly covered by moss with occasional shrubs where trees are sparse.

2.2 Methods

The fibre-optic DTS (distributed temperature sensing) system deployed in this study used makes use of Raman-scattering, optical time domain reflectometry techniques into measure measuring temperatures along the cable (Dakin et al., 1985). Scattering of incident photons from aA laser pulse within the optical fibre (SiO_2) includes generates back scatter radiation at different frequencies (Raman scattering). The system can record intensity ratios within the scatter ing spectrum (i.e., Stokes and Anti-Stokes peaks). The latter peak is highly sensitive to the temperature of the medium while the former is not (Fig. 3). The location of the temperature detected measurement is determined derived from by the travel time data (i.e., optical time domain reflectometry). Measurements were performed in dual (looped) mode wherein the laser pulse is emitted from alternate channels at each end of the cable. Calibration was performed at 0º C using a 10-m segment of the cable.

This study used a 2.7 km long fibre-optic cable (multi-mode, GI50/125, dual core; 3.4 mm, S2002A, manufactured by BRUGG, Switzerland) installed horizontally over a 2.0 km surface path (referred to as the horizontal section). Schematic illustrations of the instrument layout and experimental setup are shown in Figure 3. Temperatures were also measured at 50 cm intervals along horizontal (non-coiled) sections of the cable. Portions of the cable were also coiled around PVC tubes (effective outer diameter of 11.5 cm, and length of about 120 cm). The tubes were vertically embedded in the ground to half of their length (60 cm deep), at five stations numbered 1-5 (Fig. 2a) along the horizontal pathway. Figure 2i shows a tube prior to its installationbeing installed while Figure 2e shows a tube in operationafter installation. One loop of the coil measured about 36 cm so that three loops (*c*. 1 m) corresponded to two measurement segments (each with length ofa segment = 50 cm). This gave an effective vertical resolution of about 5 mm. Temperature data from the embedded tubes are referred to as the vertical sections.

Measurements were performed in dual (looped) mode wherein the laser pulse is emitted from alternate channels at each end of the cable. Calibration was performed at 0º C using a 10-m segment of the cable. The segment was coiled and kept in an insulated box filled with well-mixed crashed ice and water during the calibration process for about two hours.

Temperatures were also measured at 50 cm intervals along horizontal (non-coiled) sections of the cable. Measurements takenData acquired at every 10 seconds were integrated over 30-minute intervals to reduce undesirable effects of measurement error and noise. The experiment operated continuously over a two-year interval from October, 2012 to October, 2014, except for several short-period disruptions due to cable or power supply failure. Temporal monitoring was referenced to Alaskan Standard time (UTC - 9 hours).

3 Results

Figure 4 shows an example of the temperature data acquired on December 1, 2013, along a horizontal section. Figure 4a and 4b show the logarithmic ratio *r* between the anti-Stokes and Stokes components of the spectrum, and the interpreted

temperature *T* of an instantaneous measurement made at 14:30. Figure 4c illustrate the scatter between *r* and *T*. An averaged over a 24 hour period (December 1, 2013)is shown in Figure 4d along the horizontal section. The daily average tower air temperature (measured at height of 1.5 m) was -32.5º C and daily mean snow depth was 23.5 cm. In figure 4d, Downward downward spikes corresponds to temperatures of those parts of the cable exposed above the upper surface of the snow pack (minimum temperature was -32.6º C while the maximum temperature was +1.0º C). For this season, thisThe temperature difference of more than 30º C is likely due to combinations of the thermal eefects of insulation by snow pack, and of the saturation and unfrozen moisture content of the near-surface soils.

3.1 Diurnal and seasonal variation

Figure 5 shows results of DTS measurements for the six different land cover types, carried out over the two-year period. Diurnal and seasonal variations in surface temperatures indicate the influence of both microclimates and micro-environments. Land cover types co-vary with surface conditions, canopy structure, and temporal patterns at each location. In this figure, the curves in blue color indicate Figure 5 shows diurnal and seasonal temperature variation for each land cover type over the two-year period. Ddaily maximum and minimum temperatures (both in blue), and while the curve in dark blue color indicates daily average temperatures. (dark blue) from the DTS data are plotted The curves in orange and red color refer to with the JICS tower (1.5 m high) air temperatures acquired at JICS tower (1.5 m high) (orange and red, respectively). The climatological daily climatology mean temperature is overlaid in black. The blank periods (e.g., days 10-146, 165-191, and 261-295) denote valuesrefer to intervals for which missing from either DTS or tower datasets are missing. At the beginning of the 2012-2013 winter, the cable was unexpectedly accidentally severed at a point close to the DTS equipment. This event interrupted data collection along most of the cable section until the cableit could be spliced back together, after the snow melt. Section 4 discusses difficulties of using DTS equipment in taiga environments.

For the winter period (days 400-550), open moss (Fig. 5b; canopy rate=0.29, NDVI=0.592), shrub (Fig. 5c; canopy rate=0.34, NDVI=0.515), and both conifer forests types (sparse conifer in Fig. 5e; canopy rate=0.35, NDVI=0.531, and dense conifer in Fig. 5f; canopy rate=0.43, NDVI=0.495) show relatively minor variations in diurnal and daily temperatures. By contrast, thermokarst lake (Fig. 5a; canopy rate=0.46, NDVI=0.404) and deciduous forest (Fig. 5d; canopy rate=0.43, NDVI=0.239) land cover types show greater variability in daily temperatures and resume pronounced diurnal cycles relatively early on, after day 480. The ground cover for the latter two cases includes grass or limited floor vegetation, both of which are of lesser surface roughness (Figs. 2d and 2g). Differences between the two groups stem primarily from differences in snow pack characteristics. Snow pack tends to be thinner and effectively redistributed or blown by wind for the latter land cover types. Grasses are also prone to form void space between snow pack and the ground surface. Snow pack variation is further described in section 3.2 below.

In summer time (days 220 to 350, and 570 to 700), dense conifer forest exhibited daily surface temperature ranges (DTS data) less than those observed for the air column (tower observations). By contrast, open moss, shrub, and sparse forest types showed daily surface temperature ranges that were greater than those of the overlying air column. The grassy relict lake and deciduous forest land cover types showed an intermediate response. These tendencies likely reflect the openness of the canopy (or vegetation) cover above ~~at~~ the land surface (i.e., how much solar and longwave radiation reach the sensor cable), as well as local albedo of different surfaces (i.e., how much the ground surface of different land cover types reflects back). Figures 6a-6c show daily values (i.e., maximum, minimum, and average) for the DTS ~~temperature~~ anomaly relative to the corresponding tower values for days without snow cover ~~or missing values~~. Results were aggregated into four groups based on daily cloudiness, as defined by the percentage of daily total downward solar radiation between the tower (at 16-m height) and the top of the atmosphere. A box-and-whisker plot shows maximum values (100%-ile) as the top of the upper error bar, 75%-ile as the upper edge of the box, 50%-ile as the colour-coded bar, 25%-ile as the lower edge of the box, and the minimum (0%-ile) as the bottom of the lower error bar. The plot shows uniform, gradual changes in anomaly distributions from sunny days to cloudy days (Figs. 6a-6c). The size of anomaly dispersions for each land cover type (represented by the total span of the whiskers) decreases with increasing cloud cover, due to clouds' diffusing effects. Daily average temperatures at the surface generally exceed those observed by the JICS tower (at 1.5 m height). Daily maximum values appear to contribute to this effect more than do daily minimum values. The latter (daily minimum) values are closer to the tower-observed values. Among different land cover types, open moss and deciduous forest tend to give higher daily maximum and lower daily minimum anomalies.

Figures 6d and 6e show phases of diurnal extremes (i.e., exact time of either the original daily maximum or daily minimum temperature) for the DTS (colour-coded bars) and JICS tower (black line) observations, respectively. The daily maximum for surface temperatures (Fig. 6d) ~~obtains~~ are reached two hours before that of the air temperature. Relict thermokarst lake areas (grassy or bare grounds) tend to reach ~~to~~ the daily maximum temperature earlier and deciduous forest areas later than other land cover types. For the daily minimum temperature (Fig. 6e), surface and air temperatures are more in-phase with each other. This temperature ~~obtains~~ is reached in the 3rd to 4th hour (3-4 am) slot for a normal daily cycle, or at the 23rd to 24th hour (11-12 pm).

3.2 Spatial snow cover characteristics

As shown in Figure 5, snow pack greatly affects winter-time thermal conditions at the interface between the ground and snow pack. Snow cover on the ground surface strongly influences the radiative and energy budget, the water cycle, and phenology (Sturm et al., 2005; Liston, 1999; Tan et al., 2011; Immerzeel et al., 2010; Jönsson et al., 2010). Seasonal snow pack data (e.g., timing of when / how snow pack accumulates and disappears) is important for interpreting observed temperature values and for constraining energy budgets within numerical models. Snow pack is affected by the land cover types, which can amplify contrasting conditions (Liston, 1999, 2004; Sturm et al., 2005). Here, we describe how DTS data indicate different trajectories

of snow pack evolution (namely, appearance and disappearance) and produce apparent insulation effects for different land cover types.

Figure 7a shows dates of initial snow accumulation (the middle panel) and final disappearance (left and rightmost panels) for each land cover type, as counted from the date shown at the bottom of the respective panel. The presence of a continuous anow cover was defined ~~by whether~~considering the periods during which the daily amplitude in DTS temperatures fell short of 40% of that of JICS tower (1.5 m high) observations. As shown in Figure 7b, this 40% threshold effectively differentiates between snow-free and snow-covered conditions. The overall contrast between accumulation and disappearance dates (Fig. 7a) indicates that accumulation of snow cover tends to begin as spatially coherent and widespread, whereas disappearance of snow pack varies according to local conditions (Liston, 2004; Nitta et al., 2014). Among different land cover types, the majority (denoted by the margin between the 25%-ile and 75%-ile) of grassy (relict thermokarst lakes; blue) and shrubby (shrub; orange) areas vary more widely than do the forest land cover types (greens). Open moss (red) of relatively flat areas shows equal or greater variation than forest land cover types.

Another important geophysical effect of snow cover is the insulation it provides between the atmosphere and land surface. Figure 7b demonstrates this effect by showing the reduction in daily temperature range for the ground surface relative to the air. Open moss land cover shows the most spatially coherent and pronounced reduction. This implies spatial homogeneity in snow pack depth and physical properties (e.g., density, shape and size of snow grain, snow class), which could contribute to similar timing of snow disappearance (Fig. 7a). The strong insulation effect likely results from development of the depth hoar layer by radiative cooling. Relict thermokarst lake areas show high spatial variability in temperature range reduction. Forested land cover showed small reductions regardless of the ~~forest~~ vegetation types, possibly due to cooler ambient conditions beneath canopy.

3.3 Vertical temperature profiles

The fibre~~-~~optic cable wrapped around a 120 cm long, PVC tube (Fig. 8a-b) provided high-resolution vertical temperature profiles for ground, air and snow columns ~~(Fig. 8a-b)~~ at five ~~locations~~ stations each situated within different land cover types (Fig. 2a).

Station~~Location~~ #1 ~~was~~ is located~~sited~~ in dense forest, #2 in sparse forest, #3 in open moss, #4 in shrub, and #5 in a relict thermokarst lake area. Figures 8c-d show seasonal changes in daily mean temperature and temperature range respectively, for station #1~~, respectively~~. White areas represent missing values due to either cable disruption or other technical issues. Blue areas in Figure 8d show daily temperature values whose ranges are curtailed either by snowpack (above-ground for the part above the black line) or ground (below the black line). Together with Figure 8c, Figure 8d shows the different characteristics in temperature ~~structure and~~ variations between ~~in temperature regimes for~~ the air, and ~~and/or~~ snow pack ~~column~~ above the ground, and ~~during~~ between frozen or thawed periods below the ~~sub~~surface ~~conditions~~. ~~The original 30-minute data reveals thermal properties of the soil or snow media (i.e., thermal conductivity or diffusivity)~~One of the geophysical applications of

the vertical profile data is calculation of apparent thermal diffusivity. The general analytical solution of the transient conduction heat transfer equation (cf. Horton et al., 1983):

$$\partial T/\partial t = \alpha\left(\partial^2 T/\partial z^2\right), \quad (1)$$

where T is temperature, and α is thermal diffusivity ($m^2\ s^{-1}$), with a diurnal sinusoidal boundary condition, can be used to derive the ratio of the daily amplitude r between two layers of distance D as

$$r = exp\left(-\sqrt{\frac{\omega D^2}{2\alpha}}\right), \quad (2)$$

where ω is the frequency for a day. Applying Eq. (2) to the daily temperature range data (e.g, Fig. 8d) yields the distribution of the apparent thermal diffusivty (Fig. 8e. Shown in common logarithmic scale). Since it includes effects of nonconductive heat transfer such as latent heat (phase change) and convective heat transfer, it is different from true thermal diffusivity. It should also be noted that the observed diurnal cycle is not always sinusoidal. However, the calculated values clearly depict the areas of meting of snow and thawing of soil with decrease values (because of increase in apparent heat capacity due to phase change), which are smaller than the typical true thermal diffusivity values for ice (roughly, 1.15 x 10^{-6} m^2 s^{-1} at -1°C. Its common logarithm is -5.94) and water (similarly, 1.40 x 10^{-7} m^2 s^{-1} at 0°C, with its common logarithm -6.85). The Frontline of thawing soil (appeared after snow melt in both years) are evidently shown down to the depth of 20 to 25 cm, below which the attenuated diunal component in conductive heat transfer are effectively damped.

4 Technical challenges

As described above, DTS provides continuous ~~datasets~~ records suitable for ~~analysing~~ analysis of spatial variability in temperature. Data ~~continuity~~ acquisition however depends on uninterrupted functioning fibre-optic cables, uninterrupted power and communication capabilities, which in turn depend on robust equipment performance under harsh and highly variable local climate conditions. This section describes specific technical and environmental challenges identified during our study.

A continuous electrical power supply is critical for remote DTS field data collection. This requirement limits locations where DTS apparatus can be deployed. Even when available, the power system used here was subject to harsh temperature and precipitation conditions. A durable, uninterrupted power supply (UPS) is recommended for future experiments. Fibre-optic cables also pose significant logistical challenges when deployed in remote taiga forest environments. Irregular surface areas with variable moisture and numerous obstacles (such as trees) prevent construction of a simple, protected route for the cable. Deploying a ~3 km long cable from a large wooden spool, which~~,~~ together with the cable weighed more than 50 kg, around barriers and across soggy ground posed significant challenges. We chose a cable with a stainless-steel shielding tube, to optimize sensing capabilities but also protect from disruption by animals. The shielding turned out to have suboptimal flexibility (compared to that of woven stainless mesh shielding), which led to kinking and even breaking during installation. The tube-shielded cable was also too inflexible for the irregular ground surface.

A better future approach ~~to~~ for cable routing would be to use a smaller, lighter spool and shorter cable, installing the sensor as a series of shorter cable segments. A fusion splicer, already necessary for cable repair, could be used to splice shorter segments of cable in the field instead of installation of a single, long cable. Cable splicing and repair requires some training and experience, especially for performing correct core alignment under field conditions. Splicing is also not possible under harsh winter conditions (e.g., -20º C or below), even though the cable and DTS still function at these temperatures.

The DTS system is also vulnerable to cable breaks. Once the cable breaks, it cannot measure temperature beyond that point. For example, ~~If~~ if the cable breaks at 1 m of a 1 km cable system, ~~in other words,~~ the remaining 999 m will produce no data. Dual-mode measurement (a cable loop connected to two channels at both ends) can prevent total loss of measurements beyond the break, although the resulting single-mode measurements need additional calibration.

5 Summary

We deployed a fibre-optic DTS (distributed temperature sensing) system, which ~~used~~ uses ~~Raman scattering,~~techniques of optical time domain reflectometry to measure spatial and temporal variation in surface temperatures of a northern forest (taiga) site situated in Interior Alaska. The DTS system ~~consisted~~ consists of a 2.7 km fibre-optic cable, sections of which are installed on, above ~~or~~ and below surface areas ~~represented by~~with a range of different land cover types. The system provided continuous temperature ~~measurements~~ data at half-metre ~~resolution~~ distance intervals and ~~30~~ 30-minute ~~intervals~~time periods. The site, the Poker Flat Research Range (managed by the University of Alaska Fairbanks), is underlain by permafrost and primarily covered by black spruce. Land cover types of the ~~actual~~ study area ~~were classified into six categories:~~include relict thermokarst lake, open moss, shrub, deciduous forest, sparse conifer forest, and dense conifer forest. The DTS system collected data over a two-year period, from October, 2012 to October, 2014.

Data from horizontal sections of the DTS system (about 2.0 km of the cable) recorded diurnal and seasonal temperature ~~patterns~~ variations occurring in~~that varied according to~~ different land cover types and surface conditions. Snow and canopy effects for example were evident in spatio-temporal temperature patterns. Data from vertical sections (cable wrapped around PVC tubes embedded in the ground) recorded air, snow, and ground temperatures at high resolution (~5 mm).

The DTS system proved operable and useful for geophysical investigations in the harsh taiga environment, which experiences annual temperature ranges of -40º C to 30º C. However, the system also ~~demonstrated~~ faced technical challenges ~~of~~ in attempting continuous temperature measurements ~~in~~ of the ~~this~~ local environment. Future ~~research~~ activities will continue to optimize DTS systems for geoscientific research in taiga areas and other ~~harsh~~ similar environments.

Data accessibility

The DTS measurement data analysed in this paper along with ~~attributional~~ supplementary information are archived and accessible at the International Arctic Research Center (IARC) Data Archive of the University of Alaska Fairbanks (http://climate.iarc.uaf.edu/geonetwork/srv/en/main.home?uuid=60804e98-a0d5-4bcc-ab70-5d47af2b50ca).

Author contributions

KS designed and prepared the experiment. All authors took part in the tasks of ~~deployed~~ deployment of the equipment and ~~maintained~~ maintenance of the measurement system. KS prepared the manuscript with contributions from all co-authors.

Acknowledgments

This study was conducted as a part of JAMSTEC-IARC Collaboration Study (JICS). This work was partially supported by the Program for Risk Information on Climate Change (SOUSEI Program), the Integrated Research Program for Advancing Climate Models (TOUGOU program), and the Arctic Challenge for Sustainability (ArCS) program, the Japanese Ministry of Education, Culture, Sports, Science, and Technology, and by the Environmental Research and Technology Development Fund 2-1605 of the Japanese Ministry of Environment and Environmental Restoration and Conservation Agency. The Poker Flat Research Range kindly provided the facility and necessary logistics for the installments and the measurement operations. Authors gratefully acknowledge assistance from K. Noguchi, R. O'ishi, S. Matsumura, T. Nakai, Y. Igarashi, and L. Hess in installing the fibre-optic cables at the PFRR site, and NK Systems Limited for advices and guidance on the DTS settings and operations.

References

Beer, C., Lucht, W., Gerten, D., Thonicke, K. and Schmullius, C.: Effects of soil freezing and thawing on vegetation carbon density in Siberia: a modeling analysis with the Lund–Potsdam–Jena dynamic global vegetation model (LPJ-DGVM). Glob. Biogeochem. Cycle, 21, GB1012, 2007.

Dakin, J. P., Pratt, D. J., Bibby, G. W., and Ross, J. N.: Raman temperature sensor using a semiconductor light source and detector, Electronics Letters, 21(13), 569-570, 1985.

de Vrese, P., Schulz, J.-P., Hagemann, S.: On the Representation of Heterogeneity in Land-Surface–Atmosphere Coupling. *Boundary-Layer Meteorol*., 160, 157–183, 2016.

Dyer, S. D., Tanner, M. G., Baek, B., Hadfield, R. H., and Nam, S. W.: Analysis of a distributed fiber-optic temperature sensor using single-photon detectors, Optics Express, 20(4), 3456-3466, 2012.

Essery, R. L. H., Rutter, N., Pomeroy, J., Baxter, R., Staehli, M., Gustafsson, D., Barr, A., Bartlett, P., and Elder, K.: SnowMIP2: An evaluation of forest snow process simulations. Bulletin of the American Meteorological Society, 90, 1120 - 1135, doi:10.1175/2009BAMS2629.1, 2009.

Horton, R., Wierenga, P. J., and Nielsen, D. R.: Evaluation of methods for determining the apparent thermal diffusivity of soil near the soil surface. Soil Sci. Soc. Am. J. 47, 25-32, 1983.

Ikawa, H., Nakai, T., Busey, R.C., Kim, Y., Kobayashi, H., Nagai, S., Ueyama, M., Saito, K., Nagano, H., Suzuki, R., and Hinzman, L.: Understory CO2, sensible heat, and latent heat fluxes in a black spruce forest in interior Alaska. Agricultural and Forest Meteorology, 214-215, 80-90, 2015.

Immerzeel, W. W., van Beek, L. P. H., and Bierkens, M. F. P.: Climate change will affect the Asian water towers. Science, 328, 1382–1385, doi:10.1126/science.1183188, 2010.

IPCC: Climate Change 2013: The Physical Science Basis, Contribution of Working Group I to the Fifth Assessment Report of the Intergovernmental Panel on Climate Change edited by: Stocker, T. F., Qin, D., Plattner, G.-K., Tignor, M., Allen, S. K., Boschung, J., Nauels, A., Xia, Y., Bex, V., and Midgley, P. M., Cambridge University Press, Cambridge, UK and New York, NY, USA, 1535pp., 2013.

Jönsson, A.M., Eklundh, L., Hellstrom, M., Barring, L., Jonsson P.: Annual changes in MODIS vegetation indices of Swedish coniferous forests in relation to snow dynamics and tree phenology. Remote Sensing of Environment, 114, 2719-2730, 2010.

Kasurinen, V., Alfresdsen, K., Kolari, P., Mammarella, I., Alekseychik, P., Rinne, J., Vesala, T., Bernier, P., Boike, J., Langer, M., Belelli Marchesini, L., Huissteden, K., Dolman, H., Sachs, T., Ohta, T., Varlagin, A., Rocha, A., Arain, A., Oechel, W., Lund, M., Grelle, A., Lindroth, A., Black, A., Aurela, M., Laurila, T., Lohila A., and Beringer, F.: Latent heat exchange in the boreal and arctic biomes, Global Change Biology, 20, 3439–3456, doi: 10.1111/gcb.12640, 2014.

Liston, G. E.: Interrelationships among Snow Distribution, Snowmelt, and Snow Cover Depletion: Implications for Atmospheric, Hydrologic, and Ecologic Modeling, J. Applied Meteorology, 38, 1474-1487, 1999.

Liston, G. E.: Representing sub-grid snow cover heterogeneities in regional and global models. J. Climate, 17, 1381–1397, doi:10.1175/1520-0442(2004)017,1381:RSSCHI.2.0.CO;2., 2004.

Lutz, J. A., Martin, K. A., and Lundquist, J. D.: Using Fiber-Optic Distributed Temperature Sensing to Measure Ground Surface Temperature in Thinned and Unthinned Forests, Northwest Science, 86 (2), doi:10.3955/046.086.0203, 2012.

Nagano, H., Ikawa, H., Nakai, T., Matsushima-Yashima, M., Kobayashi, H., Kim, Y., and Suzuki, R.: Extremely dry environment down-regulates nighttime respiration of a black spruce forest in Interior Alaska. *Agricultural and Forest Meteorology*, 249, 297-309, doi:10.1016/j.agrformet.2017.11.001, 2017.

Nakai, T., Kim, Y., Busey, R.C., Suzuki, R., Nagai, S., Kobayashi, H., Park, H., Sugiura, K., and Ito, A.: Characteristics of evapotranspiration from a permafrost black spruce forest in interior Alaska. Polar Science, 7, 136-148, 2013.

Nitta, T., Yoshimura, K., Takata, K., Oíshi, R., Sueyoshi, T., Kanae, S., Oki, T., Abe-Ouchi, A., and Liston, G. E.: Representing Variability in Subgrid Snow Cover and Snow Depth in a Global Land Model: Offline Validation. J. Climate, 27, 3318-3330, doi:10.1175/JCLI-D-13-00310.1, 2014.

Ohta, T., Maximov, T.C., Dolman, A.J., Nakai, T., van der Molen, M.K., Kononov, A.V., Maximov, A.P., Hiyama, T., Iijima, Y., Moors, E.J., Tanaka, H., Toba, T., and Yabuki, H. Interannual variation of water balance and summer evapotranspiration in an eastern Siberian larch forest over a 7-year period (1998-2006). *Agricultural and Forest Meteorology*, **148**, 1941-1953, 2008.

Piao, S. L. et al. Net carbon dioxide losses of northern ecosystems in response to autumn warming Nature, 451, 49-U43, 2008.

Pomeroy, J., Rowlands, A., Hardy, J., Link, T., Marks, D., Essery, R., Sicart, J. E., and Ellis, C.: Spatial Variability of Shortwave Irradiance for Snowmelt in Forests. J. Hydrometeorology, 9, 1482-1490, doi:10.1175/2008JHM867.1, 2008.

Purdy, A. J., Fisher, J. B., Goulden, M. L., and Famiglietti, J. S.: Ground heat flux: an analytical review of 6 models evaluated at 88 sites and globally, J. Geophys. Res. Biogeosci., 121, doi:10.1002/2016JG003591, 2016.

Rutter, N, and 50 others, 2009. Evaluation of forest snow processes models (SnowMIP2). Journal of Geophysical Research, 114, doi:10.1029/2008JD011063Euskirchen, E. S. et al. Importance of recent shifts in soil thermal dynamics on growing season length, productivity, and carbon sequestration in terrestrial high-latitude ecosystems. Global Change Biol. 12, 731–750, 2006.

Sato, H., Kobayashi, H., Iwahana, G. and Ohta, T. Endurance of larch forest ecosystems in eastern Siberia under warming trends. *Eco.l Evol.,* **6**, 5690–5704, 2016.

Selker, J., van de Giesen, N., Westhoff, M., Luxemburg, W., and Parlange, M. B.: Fiber optics opens window on stream dynamics, Geophys. Res. Lett., 33, L24401, doi:10.1029/2006GL027979, 2006.

Selker, J. S., Thévenaz, L., Huwald, H., Mallet, A., Luxemburg, W., van de Giesen, N., Stejskal, M., Zeman, J., Westhoff, M., and Parlange, M. B.: Distributed fiber-optic temperature sensing for hydrologic systems, Water Resour. Res., 42, W12202, doi:10.1029/2006WR005326, 2006.

Sellers, P.: Modeling and observing land-surface-atmosphere interactions on large scales. *Surv Geophys*, **12**(1–3), 85–114, 1991.

Soto, M. A., Ramírez, J.A., and Thévenaz, L.: Intensifying the response of distributed optical fibre sensors using 2D and 3D image restoration, Nature Communications, 7, 10870, doi:10.1038/ncomms10870, 2016.

Sugiura, K., Suzuki, R., Nakai, T., Busey, R.B., Hinzman, L.D., Park, H., Kim, Y., Nagai, S., Saito, K., Cherry, J.E., Ito, A., Ohata, T., Walsh, J.: Supersite as a common platform for multi-observations in Alaska for a collaborative framework between JAMSTEC and IARC. *JAMSTEC Rep. Res. Dev.*, 12, 61-69, 2011.

Sturm, M., Schimel, J., Michaelson, G., Welker, J. M., Oberbauer, S. F., Liston, G. E., Fahnestock, J., and Romanovsky, V. E.: Winter Biological Processes Could Help Convert Arctic Tundra to Shrubland, BioScience, 55(1):17-26. 2005.

Tan, A., Adam, J. C., and Lettenmaier, D. P.: Change in spring snowmelt timing in Eurasian Arctic rivers. J. Geophys. Res., 116, D03101, doi:10.1029/2010JD014337, 2011.

Thomas, C. K., Kennedy, A. M., Selker, J. S., Moretti, A., Schroth, M. H., Smoot, A. R., Tufillaro, N. B., Zeeman, M. J.: High-Resolution Fibre-Optic Temperature Sensing: A New Tool to Study the Two-Dimensional Structure of Atmospheric Surface-Layer Flow, Boundary-Layer Meteorol., 142, 177–192, doi:10.1007/s10546-011-9672-7, 2012.

Tyler, S. W., Selker, J. S., Hausner, M. B., Hatch, C. E., Torgersen, T., Thodal, C. E., and Schladow, S. G.: Environmental temperature sensing using Raman spectra DTS fiber-optic methods, Water Resour. Res., 45, W00D23, doi:10.1029/2008WR007052, 2009.

5

Figure 1: Location of the DTS system installed at the Poker Flat Research Range (PFRR; University of Alaska Fairbanks).

Figure 2: (a) Layout of the fibre-optic cable sensor (black line) installed at the PFRR with stations numbered from 1 to 5 (in white), together with the land cover types designated from satellite images (dark blue: relict thermokarst lake, red: open moss, orange: shrubs, light green: deciduous forest, green: sparse conifer forest, blue: dense conifer forest). (b) Frequency of land cover types along the cable. (c) Scatter plot of surface-measured canopy rate and satellite-derived normalized difference vegetation index (NDVI; GeoEye1 image taken on Sept. 25, 2010). Images show examples of (d) relict thermokarst lake, (e) open moss, (f) shrub, (g) deciduous forest, (h) sparse conifer forest, and (i) dense conifer forest.

Figure 3: Schematics of schematic illustrations of instrument layout and experimental setup~~Raman scattering~~.

Figure 4: Examples of outputs from the DTS equipment. a) The logarithmic ratio between the Stokes and anti-Stokes components and b) temperature of an instantaneous measurement (made at 12:00 on December 1, 2013) for a horizontal section of the DTS system. c) Scatter plot between a) and b). d) Average of the temperature measurements for the day~~distribution measured by a horizontal section of the DTS system (daily mean for December 1, 2013)~~.

Figure 5: Typical seasonal variations in daily temperatures for the six land cover types: (a) relict thermokarst lake, (b) open moss, (c) shrub, (d) deciduous forest, (e) sparse conifer forest, and (f) dense conifer forest. Plot shows daily maximum and minimum temperatures from the DTS system (blue lines) and the JICS tower (air column at 1.5 m height; orange lines) along with daily mean values (dark blue for DTS and red for the JICS tower). The black line shows daily climatology. Data span time period after October 13, 2012.

Figure 6: Distributional differences between (a) daily maximum temperatures, (b) daily minimum temperatures, and (c) daily average temperature under different degrees of cloudiness (32 observations for 0-25%, 69 observations for 25-50%, 80 observations for 50-75%, and 5 observations for 75-100%). Lower plots show median maximum (d) and minimum (e) temperature values and frequency (total hours) as measured by DTS for land cover types (colour-coded) compared to corresponding values from the JICS tower (1.5 m height; black-line histogram).

Figure 7: (a) Differences in snow melt (or accumulation) dates for different land cover types for the spring of 2013 (after April 21, 2013), autumn of 2013 (after October 19, 2013), and spring of 2014 (after April 1, 2014). (b) Damping rate for daily temperature range averaged over snow-covered days having continuous measurements (i.e., without missing or interrupted cable data) for the 50-day period following the respective start date of the season.

Figure 8: Subsurface and above-surface temperatures measured by vertical sections. (a) Photo of PVC tube with sensor cable wrapping prior to installation. (b) Photo of PVC tube with temperature sensor (vertical section) installed within a dense conifer forest. Depth-time ~~cross-section~~profiles for (c) daily mean temperatures and (d) daily temperature range during 2013 snow melt period. (e) same as (c) except for apparent thermal diffusivity [m^2 s^{-1}], shown in common logarithmic scale.

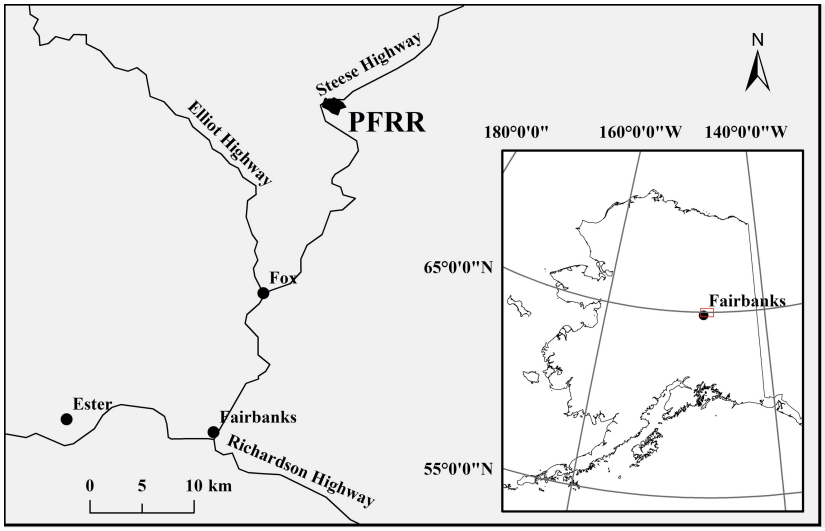
Steese Highway
Elliot Highway
PFRR
Fox
Ester
Fairbanks
Richardson Highway
0 5 10 km
N
180°0'0"
160°0'0"W
140°0'0"W
65°0'0"N
55°0'0"N
Fairbanks

Fig01

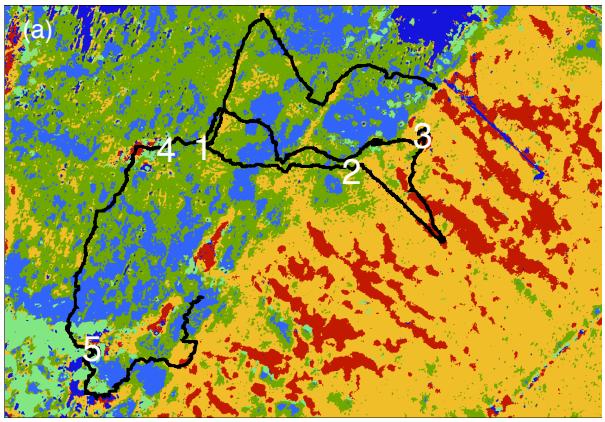
(a)
1
2
3
4
5

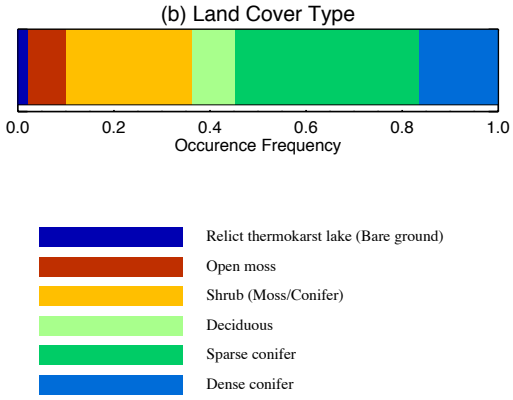
(b) Land Cover Type
0.0
0.2
0.4
0.6
0.8
1.0
Occurence Frequency
Relict thermokarst lake (Bare ground)
Open moss
Shrub (Moss/Conifer)
Deciduous
Sparse conifer
Dense conifer

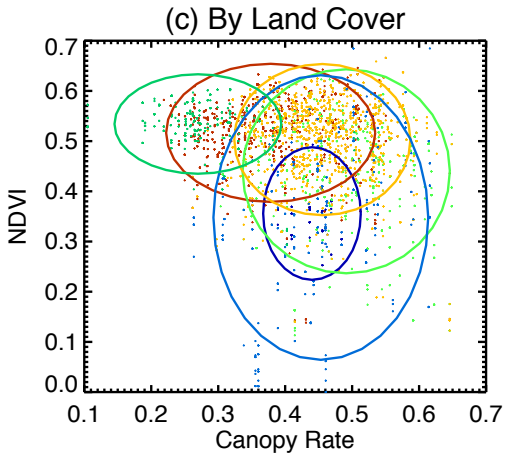
(c) By Land Cover
NDVI
0.0
0.1
0.2
0.3
0.4
0.5
0.6
0.7
Canopy Rate

Fig02

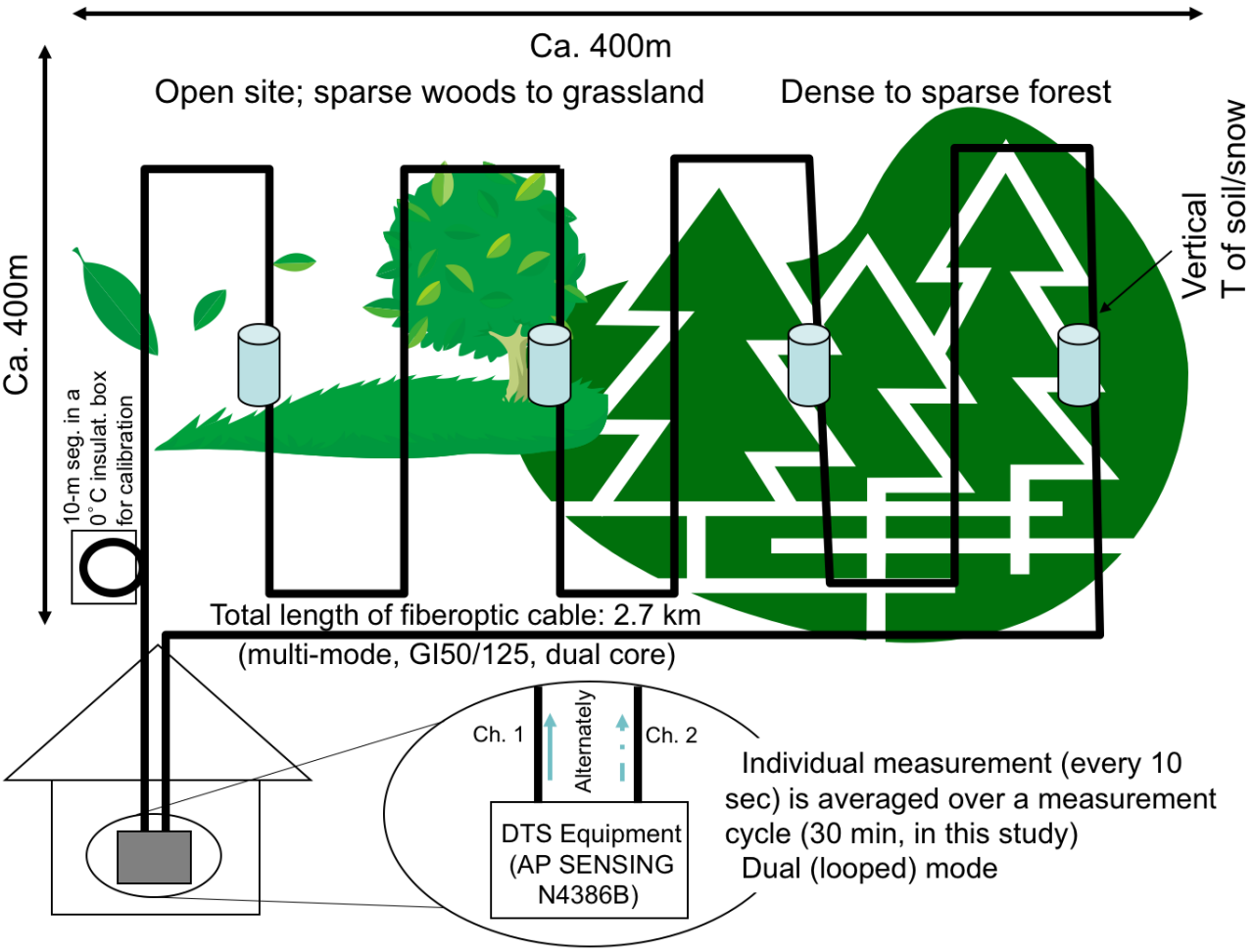
Ca. 400m
Open site; sparse woods to grassland
Dense to sparse forest
Ca. 400m
Vertical
T of soil/snow
10-m seg. in a
0 °C insulat. box
for calibration
Total length of fiberoptic cable: 2.7 km
(multi-mode, GI50/125, dual core)
Ch. 1
Alternately
Ch. 2
DTS Equipment
(AP SENSING
N4386B)
Individual measurement (every 10
sec) is averaged over a measurement
cycle (30 min, in this study)
Dual (looped) mode

Fig03

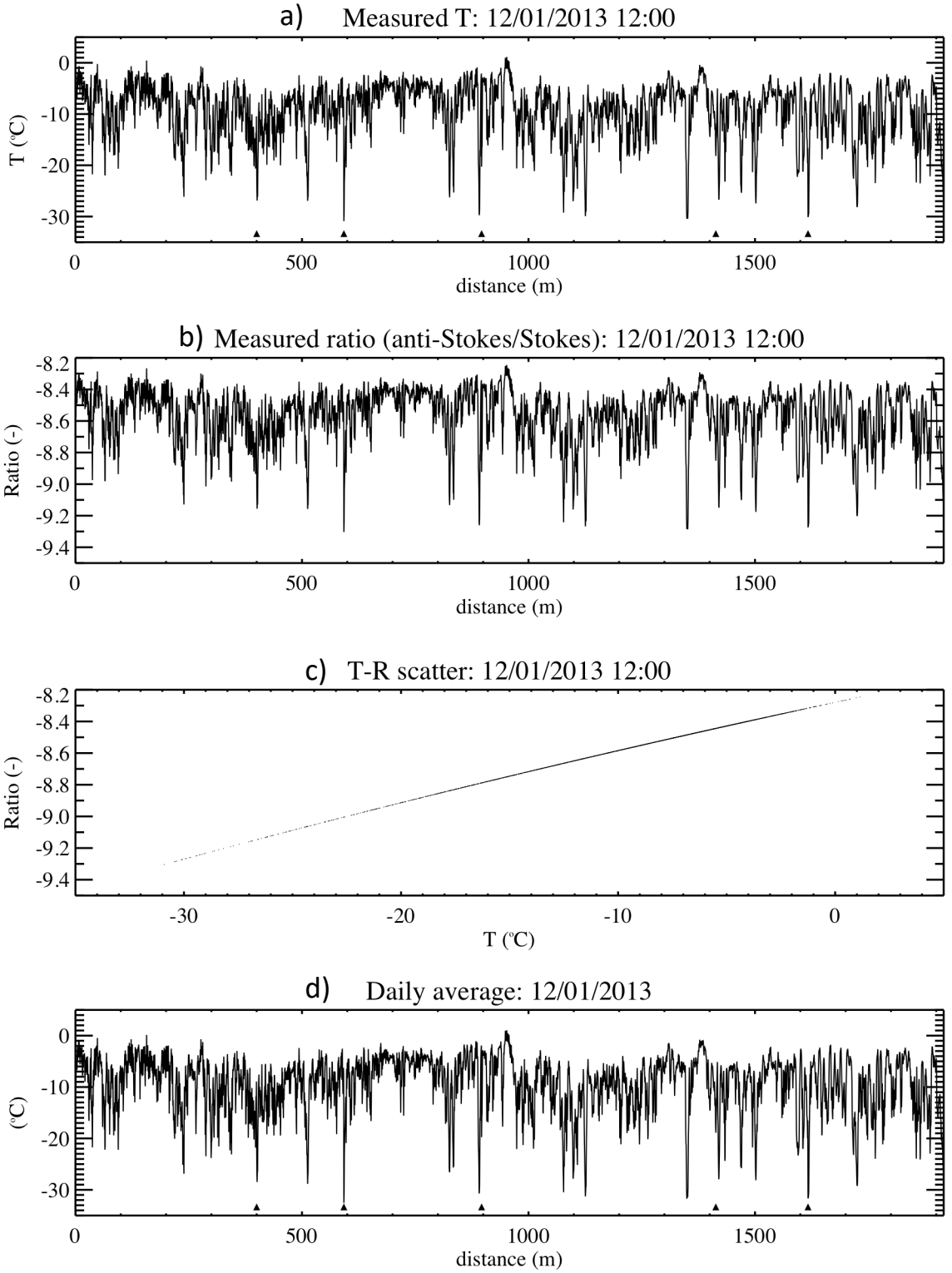
a) Measured T: 12/01/2013 12:00
T (°C)
0
-10
-20
-30
0
500
1000
1500
distance (m)
b) Measured ratio (anti-Stokes/Stokes): 12/01/2013 12:00
Ratio (-)
-8.2
-8.4
-8.6
-8.8
-9.0
-9.2
-9.4
0
500
1000
1500
distance (m)
c) T-R scatter: 12/01/2013 12:00
Ratio (-)
-8.2
-8.4
-8.6
-8.8
-9.0
-9.2
-9.4
-30
-20
-10
0
T (°C)
d) Daily average: 12/01/2013
(°C)
0
-10
-20
-30
0
500
1000
1500
distance (m)

Fig04

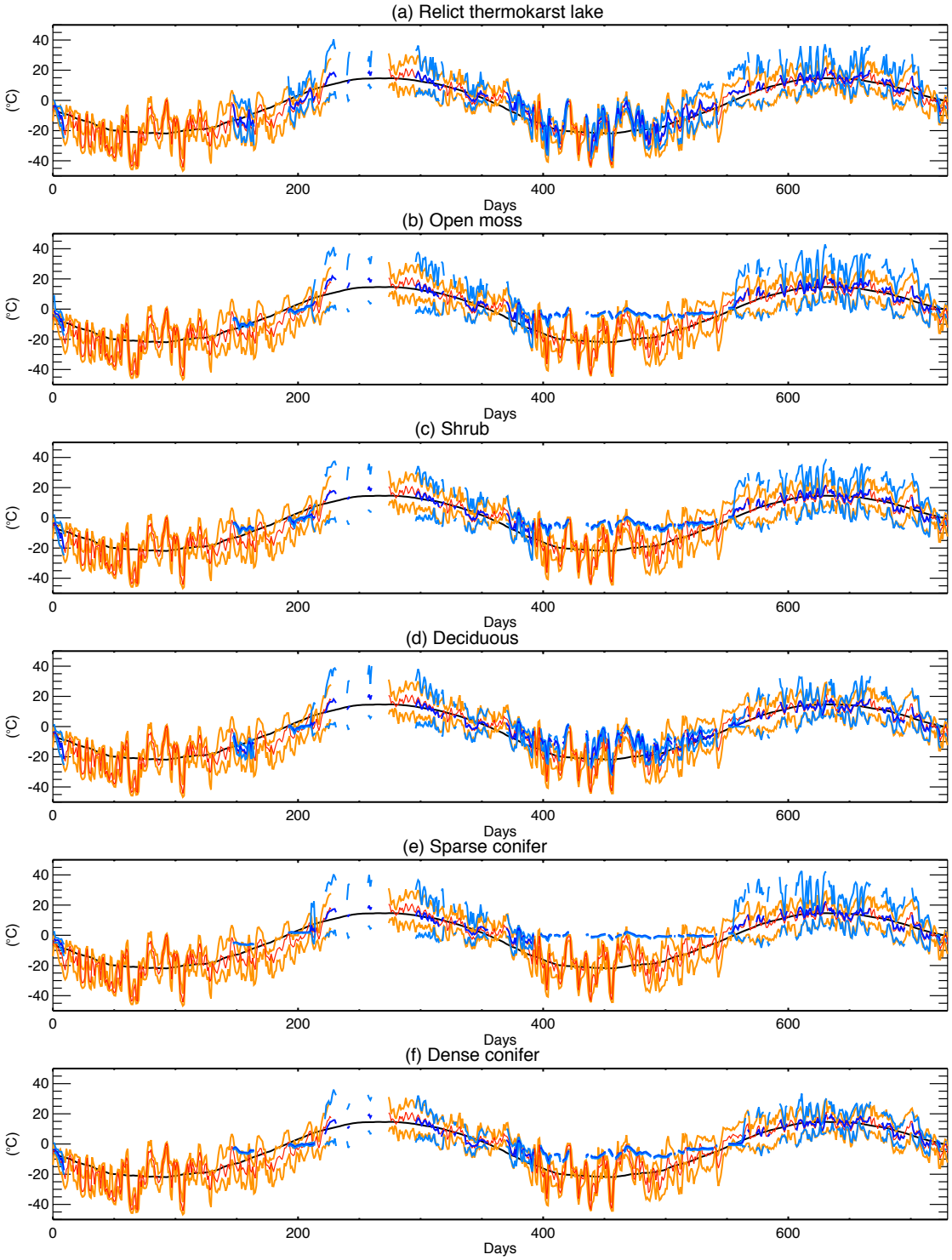
(a) Relict thermokarst lake
(b) Open moss
(c) Shrub
(d) Deciduous
(e) Sparse conifer
(f) Dense conifer
(°C)
Days
40
20
0
-20
-40
0
200
400
600

Fig05

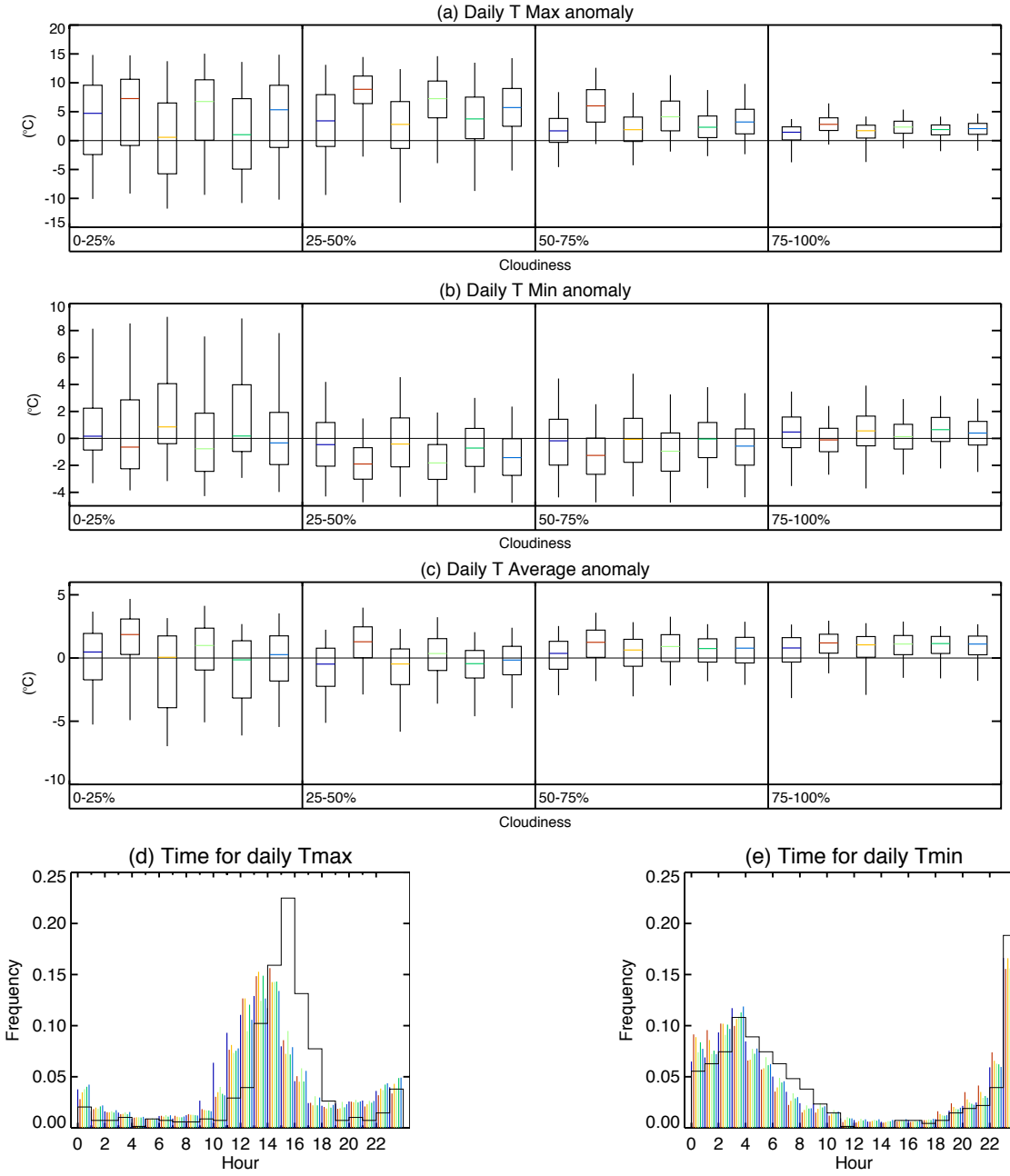
(a) Daily T Max anomaly
(°C)
0-25%
25-50%
50-75%
75-100%
Cloudiness
(b) Daily T Min anomaly
(°C)
0-25%
25-50%
50-75%
75-100%
Cloudiness
(c) Daily T Average anomaly
(°C)
0-25%
25-50%
50-75%
75-100%
Cloudiness

(d) Time for daily Tmax
Frequency
Hour
(e) Time for daily Tmin
Frequency
Hour

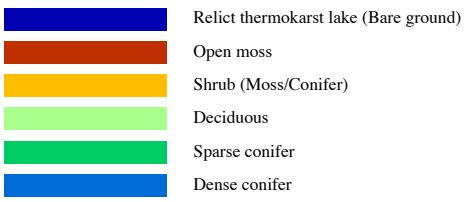
Relict thermokarst lake (Bare ground)
Open moss
Shrub (Moss/Conifer)
Deciduous
Sparse conifer
Dense conifer

Fig06

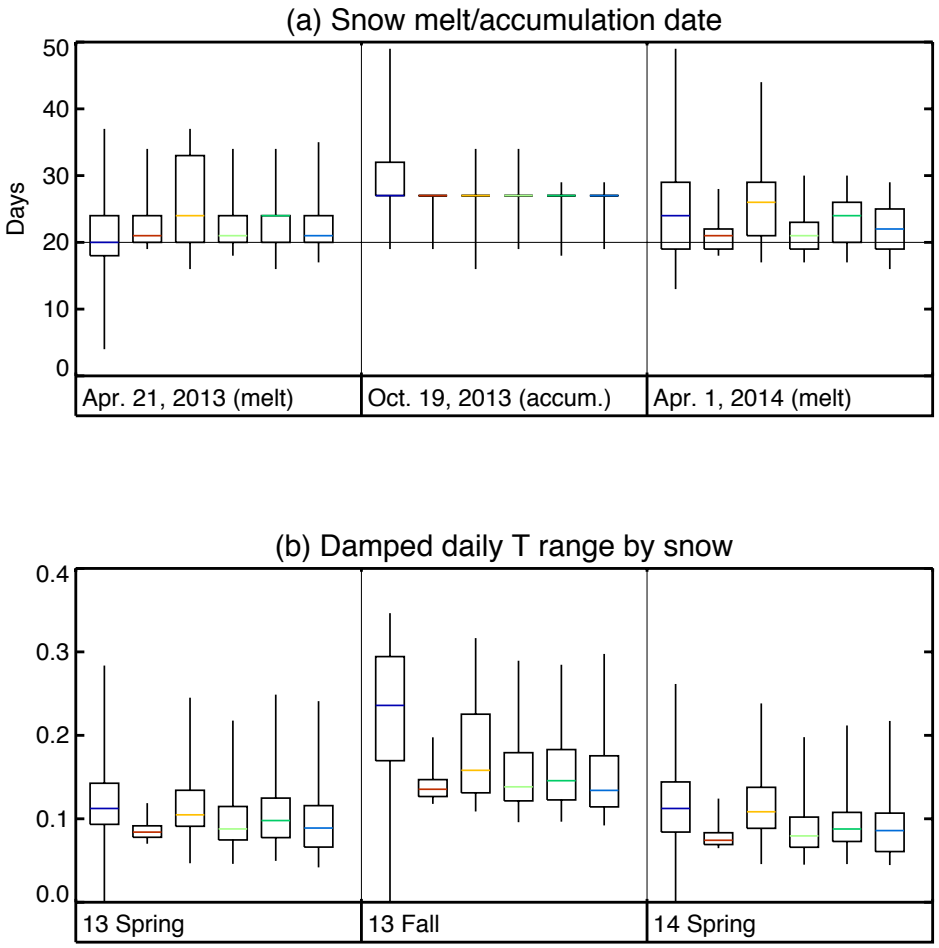
(a) Snow melt/accumulation date
Days
50
40
30
20
10
0
Apr. 21, 2013 (melt)
Oct. 19, 2013 (accum.)
Apr. 1, 2014 (melt)
(b) Damped daily T range by snow
0.4
0.3
0.2
0.1
0.0
13 Spring
13 Fall
14 Spring
Relict thermokarst lake (Bare ground)
Open moss
Shrub (Moss/Conifer)
Deciduous
Sparse conifer
Dense conifer

Fig07


(a)


(b)

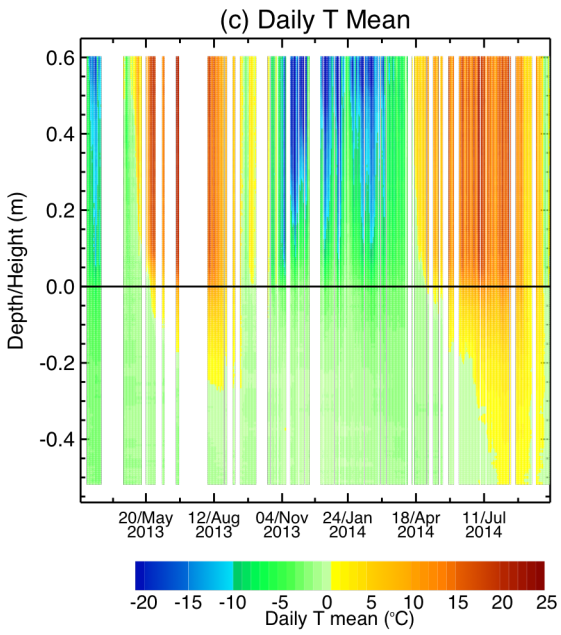
(c) Daily T Mean
Depth/Height (m)
0.6
0.4
0.2
0.0
-0.2
-0.4
20/May 2013
12/Aug 2013
04/Nov 2013
24/Jan 2014
18/Apr 2014
11/Jul 2014
-20 -15 -10 -5 0 5 10 15 20 25
Daily T mean (°C)

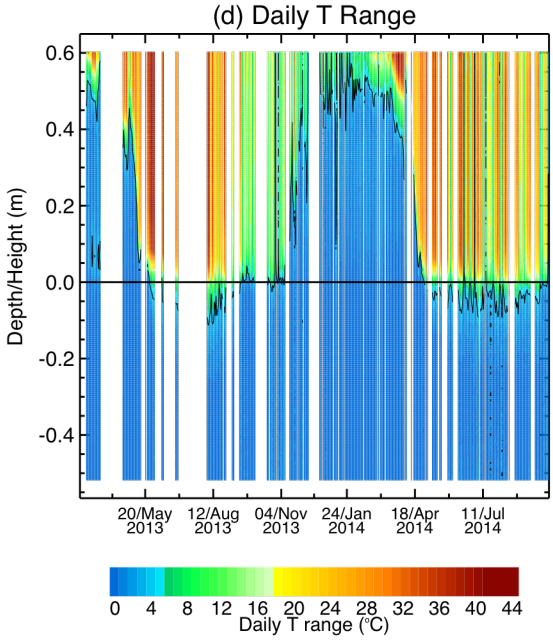
(d) Daily T Range
Depth/Height (m)
0.6
0.4
0.2
0.0
-0.2
-0.4
20/May 2013
12/Aug 2013
04/Nov 2013
24/Jan 2014
18/Apr 2014
11/Jul 2014
0 4 8 12 16 20 24 28 32 36 40 44
Daily T range (°C)

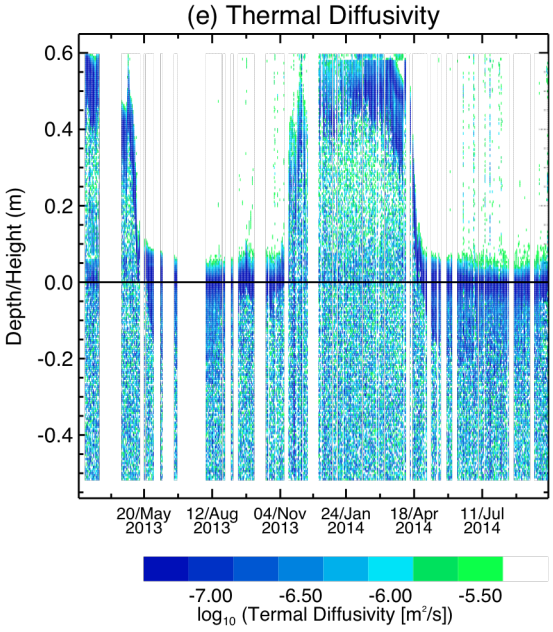
(e) Thermal Diffusivity
Depth/Height (m)
0.6
0.4
0.2
0.0
-0.2
-0.4
20/May 2013
12/Aug 2013
04/Nov 2013
24/Jan 2014
18/Apr 2014
11/Jul 2014
-7.00 -6.50 -6.00 -5.50
log10 (Termal Diffusivity [m²/s])

Fig08